IEEE Access
Multidisciplinary | Rapid Review | Open Access Journal

Received December 9, 2020, accepted December 20, 2020, date of publication December 25, 2020, date of current version January 7, 2021.

Digital Object Identifier 10.1109/ACCESS.2020.3047461

3-D Block-Rooting Scheme With Application to Medical Image Enhancement

VIACHESLAV VORONIN[1], (Member, IEEE), ALEKSANDER ZELENSKY[1], AND SOS AGAIAN[2], (Fellow, IEEE)

[1]Center for Cognitive Technology and Machine Vision, Moscow State University of Technology "STANKIN," 127055 Moscow, Russia
[2]Department of Computer Science, The City University of New York, New York, NY 10314, USA

Corresponding author: Viacheslav Voronin (voroninslava@gmail.com)

This work was supported by the Russian Ministry of Science and Education for support under the grant for conducting basic scientific research by educational organizations in 2020-2022 under Project NoFSFS-2020-0031.

ABSTRACT The goal of image enhancement is to improve certain features and details on an image. It is a critical procedure in image processing (image segmentation, feature extraction), medical imaging (such as X-ray, CT, and MRI) and computer vision (target, object, and text detection; segmentation, registration, and recognition). X-ray, CT, and MRI images are often affected by blurriness and lack of contrast, but the clarity of these images is very important for the accuracy of medical diagnosis and treatment. This article offers (1) a 3-D transform block-rooting scheme-based image enhancement method and (2) a non-reference transform-domain quality measure to choose the presented algorithm parameters optimally. Experimental results from NYU, fastMRI, and ChestX-ray data sets show that the proposed technique performs well and can reduce noise during the sharpening of the image details. At the same time, it can undoubtedly be used in different medical image processing systems.

INDEX TERMS Image enhancement, 3-D block-matching, medical imaging, MRI, transform-domain, non-reference quality measure, alpha-rooting, Fourier transform.

I. INTRODUCTION

Medical images, satellite images, and even real-life photographs may suffer from different degradations, such as low contrast [1]. This can be due to poor illumination, the finite sensitivity of the imaging device, electronic sensor noise, or atmospheric disturbances that lead to broadband noise. Image enhancement has been widely used for security purposes [2], military operations [3], human activity recognition, medical diagnoses [4], and more [5]–[9]. Image enhancement refers to processing images to make them more suitable for display or further image analysis [7]. So, image enhancement is a problem-oriented procedure for improving the visual appearance of the medical image. The presented method provides tools for a future automated image-processing (analysis, detection, segmentation, and recognition) system [10].

Furthermore, significant difficulty in this endeavor is the lack of assessment procedures to assess and compare various effectiveness methods' enhancement. The clear visual quality of medical images (e.g., X-ray, MRI, CT) is necessary for the interpretability or perception of information in the image for human viewers [11]. In most cases, the pixel intensity of medical images has poor contrast, making the distinguishability of objects more complicated (Fig. 1). Generally, the interpretations of medical images are examined by medical professionals [12]. This is wholly limited due to its subjectivity and the complexity of the medical images [13]. Besides, there are significant variations between experts, and fatigue often sets in due to their heavy workload.

This article focuses on the problems associated with medical-image enhancement by using a 3-D block-rooting scheme. The primary contributions of our article include a novel:

1) 3-D block-rooting scheme tailored to medical image enhancement application by using local and global image information;
2) Boundary consistency and artifacts elimination method based on sparse collaborative transform domain representation;
3) Golden transform-domain based non-reference image quality assessment for choosing the best Algorithm's parameters driven from medical image properties.

The associate editor coordinating the review of this manuscript and approving it for publication was Chao Zuo.

This work is licensed under a Creative Commons Attribution 4.0 License. For more information, see https://creativecommons.org/licenses/by/4.0/

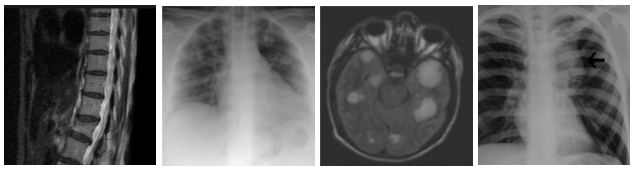

FIGURE 1. Medical images.

This article is organized in the following manner: Section II presents the image enhancement background information. Section III defines an image enhancement algorithm by using a new 3-D block-matching scheme. Section IV lays out the proposed enhancement quality measure. Section V presents some results for choosing the parameters of the proposed method-driven optimization enhancement quality measure. Section VI presents extensive computer simulation results. Finally, Section VII gives some concluding comments.

II. RELATED WORK

Image enhancement technology can be categorized into two classes: spatial and frequency domain methods [8]. The first group uses a spatial domain image processing base on linear or nonlinear operations that directly manipulate the pixels [1]. The shape of the histogram of an image provides useful info about the possibility of contrast enhancement. Many spatial image enhancement methods are based on histogram analysis and modification: histogram equalization, histogram matching, contrast stretching, intensity adjustment, etc. [10], [14]–[17].

One of the most popular image enhancement methods is histogram equalization [18]. It is a global processing approach, so the entire tone of the image has been changed, like a brighter or darker image. In many cases, these methods extend the dynamic range of an image in local regions, leading to artifacts and overall tonal change of the image [1].

The histogram equalization (HE) [18], adaptive histogram equalization (AHE) [19], and contrast-limited adaptive histogram equalization algorithm (CLAHE) [16] are the classical spatial domain methods which manipulate the histogram of the image to be uniformly distributed [7]. If an image has large peaks in the histogram, it leads to over enhancement. AHE is the method for considering local information during image enhancement, which can highlight the details and textures. This approach often amplifies the noises in uniform image areas [20]. The CLAHE algorithm and its modifications [16], [21], [22] limit each sub-block histogram and make the image contrast more natural. However, this method produces ring artifacts on edges [8]. Other image enhancement algorithms modify brightness using bi-histogram equalization (BBHE) [23] and adaptive gamma correction weighting distribution (AGCWD) [24].

BBHE equalizes the two sub-images separately to maintain the brightness of the image. AGCWD modifies histograms and enhances contrast in images using a weighted distribution function [23]. This operation increases the low intensity and avoids decrement of the high intensity of the brightness. In cases where there are several peaks in the histogram, this method may cause many details of the bright areas of the image to be lost [7] and often provides unsatisfactory results because they cannot take full advantage of local data.

In [25] the authors built CID2013 and CCID2014 datasets and introduced the contrast enhancement method based on phase congruency and information statistics of the image histogram. Also, K. Gu *et al.* proposed an enhancement algorithm via machine learning [26]. Another enhancement technology with saliency preservation was devised by taking account of the fact that adequately enhanced images should be entropy increment and saliency preservation [27].

The widely used image enhancement techniques include log transform, gamma transform, and fuzzy method [10], [28]–[34]. The Retinex algorithms are developed for color constancy [35]–[37]. These algorithms use the color image model based on the estimation of the reflectances of each point by calculating the relative light and shade relations. This Algorithm is improved and appears as a multiscale Retinex [38]. In essence, all these algorithms smooth the image through the Gaussian model and extract the image's background.

Alpha-rooting is one of the more popular frequency domain enhancement methods [1], [11], [39], [40]. It uses transformation in the frequency domain through modification magnitudes and altering the frequency content of the image. This method's basic limitation as global processing is that it cannot enhance all parts of the image. Besides, these enhancement techniques use frequency transformations, such as DCT, Fourier, and the following types of processing: *alpha*-rooting, frequency filtering, homomorphic filtering, etc. [4], [8], [41].

So, the weaknesses of traditional methods are: 1) being extremely sensitive to parameters; 2) failing to enhance irregular lighting and brightness gradients; 3) for point processing spatial information completely lost; 4) a global processing approach has been changing the entire tone of the image like the more bright or dark image; 5) extending the dynamic range of an image in local regions, which leads to artifacts and an overall tonal change in the image; and 6) frequency domain methods introduce certain artifacts called "objectionable blocking effects," and they cannot simultaneously enhance all parts of the image very well.

At present, global contrast enhancement usually excessively enhances the brighter local areas, resulting in the diffusion of the high-luminance regions of the image and the loss of details in high-illumination regions [42]. Local contrast enhancement provides more considerable contrast enhancement in the areas of interest. However, it brings poor effect for dark detail enhancement and usually has more noise points, reducing visual comfort. The contrast enhancement for low-illumination gray images with nonuniform illumination is always a challenge in image processing, which lacks a robust algorithm to solve the problem.

Most global transform domain methods may introduce some artifacts by enhancing the background noise, may over-enhance and under-enhance images, may not work well

on irregular lighting and brightness images, and may not preserve the local image features/details. This article presents a new block-rooting enhancement scheme using local and global image information for medical diagnosis, treatment, and clinical research.

III. 3-D BLOCK-MATCHING SCHEME AND IMAGE ENHANCEMENT ALGORITHM

This article presents a new image enhancement algorithm based on combined local and global image processing. The flowchart of the proposed enhancement algorithm is shown in Figure 2.

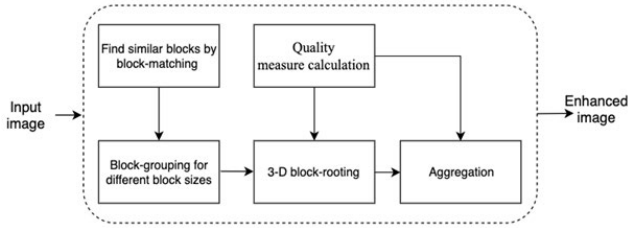

FIGURE 2. Flowchart of the proposed image enhancement method.

The proposed technique uses the block-matching for square patches grouping and the block-rooting in a 3-D transform domain. The algorithm includes the following main steps: 1) block splitting using extraction blocks with different sizes from the input image; 2) block matching via search similar blocks to the reference one and combine them to the 3-D group; 3) perform 3-D block-rooting and return the estimates to their original locations, and 4) choose the best (optimal) enhancement image through optimization of the proposed enhancement measure.

The whole image's final estimation is calculated as a weighted average of all overlapping obtained block estimates after processing all reference blocks.

A. NOVEL 3-D BLOCK-ROOTING SCHEME

This article presents a new image enhancement algorithm based on combined local and global image processing (Fig. 4). We realize grouping by block-matching within the enhanced image Z, as discussed in Section III-A.

This general procedure of 3-D block-matching is illustrated in Figure 3 and proceeds as Algorithm 1.

Block-Splitting: We using extraction blocks with different sizes from the input image. The sizes of the blocks are 8 by 8, 16 by 16, 32 by 32, and, i.e., For this purpose, we move the square block from up left corner to down right corner with step equal one.

Definition 1: By blocks splitting, we mean the dividing of the image into fixed-sized blocks.

Grouping: We find blocks that are similar to the current for every size processed one and then stacked them together in a 3-D array (group) [43]. We consider similar blocks for whom Euclidean distance with respect to the reference block is smaller than a fixed threshold.

Algorithm 1 3-D Block-Rooting

For each block Z_{x_R} in the image, do the following
1. Block-splitting.
2. Block-grouping.
3. Collaborative block-rooting.
4. Aggregation.

$\tilde{Z}_{x_R}$ is the output image block.

Algorithm 2 Block-Splitting-Grouping Algorithm

Input: An image Z.
1. Split the image into $k \times k$ blocks Z_x.
2. Take a distance d, for example, the Euclidean distance.
3. Take a "reference" block Z_{x_R} and a threshold τ^{ht}_{match}.
4. Compute the distance $d(Z_{x_R}, Z_x)$.
5. Stack all blocks together with $d(Z_{x_R}, Z_x) \leq \tau^{ht}_{match}$ and form 3-D block.

Output: Formed 3-D block by grouping by the block Z_{x_R}.

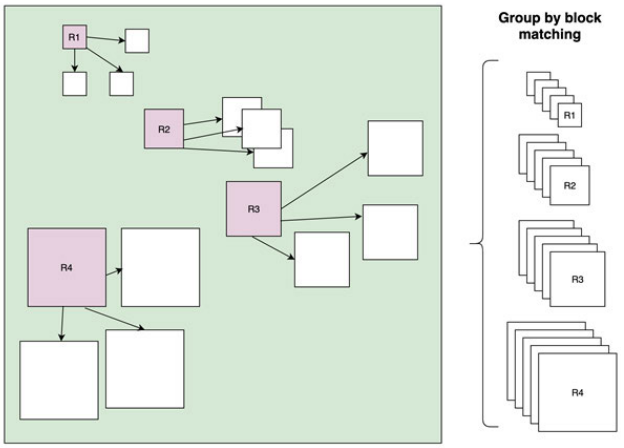

FIGURE 3. Diagram of the 3-D block-matching scheme.

The procedure for the proposed block-splitting and grouping algorithm is expressed in the steps below.

Collaborative Block-Rooting: A 3-D Fourier transform is applied to the formed group, enhanced every block by alpha-rooting. So, a collaborative transform-based enhancement algorithm base on the α-rooting and magnitude reduction method in the 3-D transform domain. After this, we invert the 3-D transform and return the estimates of the blocks to their original positions.

Definition: Block-rooting is the *alpha*-rooting method applied to group blocks in 3-D Fourier transform.

This procedure proceeds as Algorithm 3.

Aggregation: Compute the primary estimate of the true-image by weighted averaging all of the obtained overlapping block-wise estimates.

B. NOVEL BLOCK-ROOTING METHOD USING 3-D BLOCK-MATCHING SCHEME

Suppose $Z \in \mathbb{C}^{I_1 \times I_2 \times I_3}$ is an 3^{th} order complex-valued tensor for original signal. Its 3-dimensional discrete Fourier

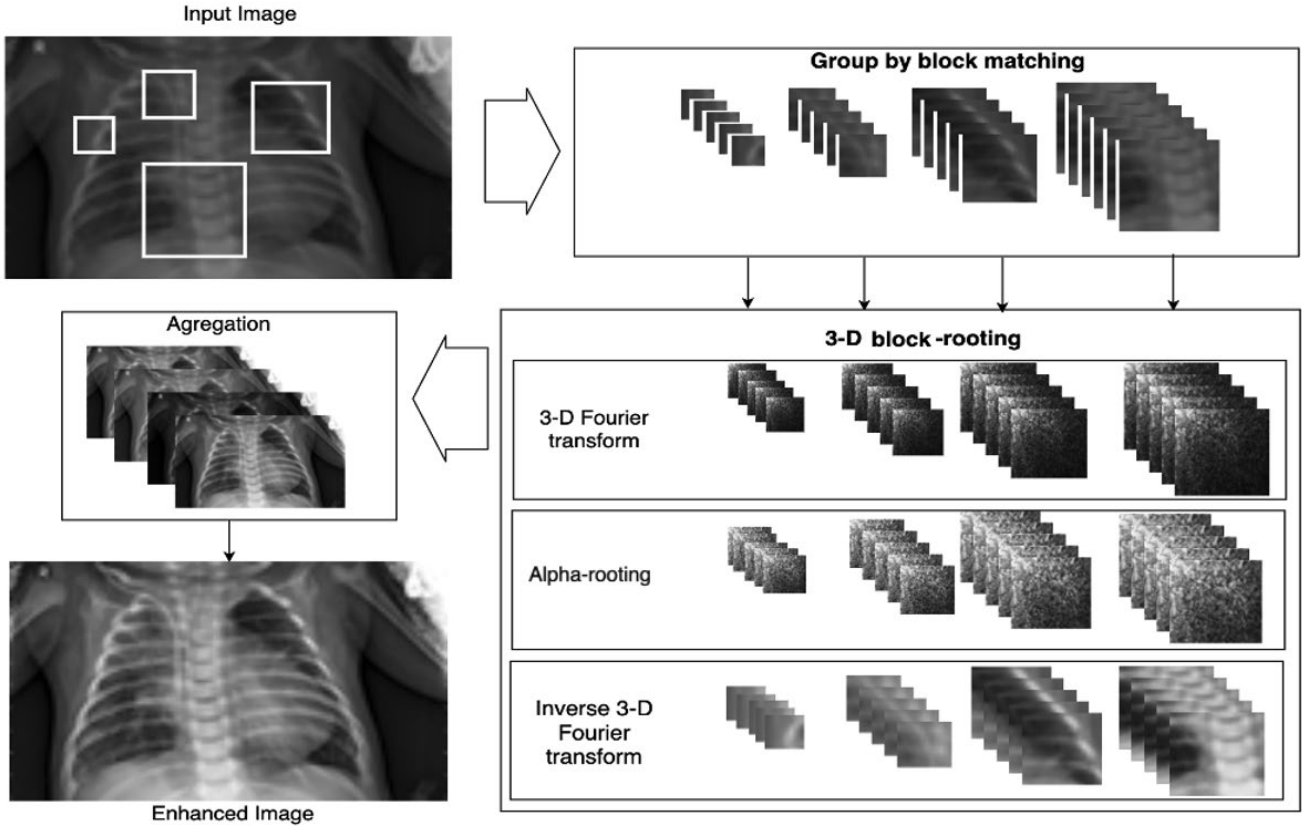

FIGURE 4. Block-rooting method using 3-D block-matching scheme.

Algorithm 3 Collaborative Block-Rooting

Input: An image Z.

1. Formed 3-D block using the block grouping algorithm.
2. Apply a 3-D Fourier transform on the formed group.
3. Perform the alpha-rooting algorithm on Fourier transform coefficients.
4. Apply the inverse 3-D Fourier transform on modified by alpha-rooted coefficients.
5. Return the enhanced blocks-images to their original positions.

Output: Collaborative block-rooted enhanced image $\tilde{Z}$.

transform $\in \mathbb{C}^{I_1 \times I_2 \times I_3}$ can write as

$$Y(j_1, j_2, j_3) = \sum_{n_1=1}^{N_1-1} \sum_{n_2=1}^{N_2-1} \sum_{n_3=1}^{N_3-1} Z(n_1, n_2, n_3) \times exp\left(-i\frac{2\pi}{N_1} n_1 j_1 - i\frac{2\pi}{N_2} n_2 j_2 - i\frac{2\pi}{N_3} n_3 j_3\right),$$

where N_1, N_2, and N_3 are the amount of the number in every dimensionality; i is the imaginary unit.

In tensor notation, the summation can be expressed with successive k-mode products which is defined as

$$B = A \times_k U \Leftrightarrow \mathrm{B}(i_1, i_2, i_3) = \sum_{i_k=1}^{I_3} U(j, i_k) A(i_1, i_2, i_3)$$

for any $A \in \mathbb{C}^{I_1 \times I_2 \times I_3}$ and $U \in \mathbb{C}^{J \times I_k}$ yielding $B \in \mathbb{C}^{I_1 \times I_2 \times I_3}$.

The 3-dimensional discrete Fourier transform can be written as

$$Y = Z \times_1 F_{I_1} \times_2 F_{I_2} \times_3 F_{I_3}.$$

where $F_{I_k}(n_k, j_k) = exp\left(-i\frac{2\pi}{N_k} n_k i_k\right)$, $\forall k \in \{1, 2, 3\}$ with i being the imaginary unit.

Vectorization of each side results in $y = vec(Y), z = vec(Z)$ then $y = (F_{I_3} \otimes F_{I_2} \otimes F_{I_1}) z$, where $\otimes$ is Kronecker product. We apply a 3-dimensional discrete Fourier transform for every image sets of the blocks, so realized grouping by block-matching within the image Z [43]. We only use blocks whose distance with respect to the reference block is smaller than a fixed threshold and is considered to be similar and grouped. The Euclidean distance as a measure of dissimilarity is considered. The number of blocks is fixed and equal to 8. The block distance could be calculated as

$$d(Z_{x_R}, Z_x) = \frac{\left\| Z_{x_R} - Z_x \right\|_2^2}{(N_1)^2},$$

where N_1 is the size of the window; $d = 2$ denotes the Euclidean-norm and the blocks Z_{x_R} and Z_x are respectively located at x_R and x in Z.

In most cases, some random noise is present on the image, which obstructs the correct determination of similar blocks. To decide this problem, we use pre-filtering

for a block-similarity measure calculation [43]. The hard thresholding applied to Fourier coefficients on both blocks, which results in $d(Z_{x_R}, Z_x)$, as shown at the bottom of the page. where $\mathfrak{F}^{ht}_{2D}$ is the hard-thresholding operator with threshold λ_{thr}.

Naturally, Υ is defined as

$$\Upsilon(\lambda, \lambda_{thr}) = \begin{cases} \lambda, & if\ |\lambda| > \lambda_{thr} \\ 0, & otherwise. \end{cases}$$

In this way, we receive the coordinates of the blocks that are similar [40]:

$$S^{ht}_{x_R} = \left\{ x \in X : d(Z_{x_R}, Z_x) \le \tau^{ht}_{match} \right\},$$

where the τ^{ht}_{match} is the maximum distance for blocks similarity measure.

For the proposed image enhancement method, we use the frequency domain. One simply performs the transformation of the image to be enhanced, then manipulates the transform coefficient, and then performs the inverse orthogonal transform. The linearly or non-linearly modification of the spectral coefficients can be used for enhancement and visualization. So, a transform-based enhancement algorithm base on the α-rooting and magnitude reduction method. The collaborative 3-D block-rooting is realized by transforming Fourier coefficients in the 3-D transform domain. The adopted normalized 3-D linear transform denoted as $\mathfrak{F}^{ht}_{3D}$, is expected to take advantage of the correlation and attain good sparsity for the signal group.

For every block, we use a transform-based enhancement algorithm based on the α-rooting and magnitude reduction method [1], [4]:

$$\tilde{Z}_{x_R}(p, s) = \left| Z_{x_R}(p, s) \right|^{\alpha} \cdot e^{i\theta(p,s)},$$

where $Z_{x_R}(p, s)$ is the transform coeffcients of the image, α is a user defined operating parameter, $\theta(p, s)$ is the phase of the transform coefficients.

This allows for effective block enhancement, followed by an inverse transform that yields a 3-D array of block-wise estimates. The procedure for the proposed algorithm is expressed in the steps below.

For every patch of the image, we apply the α-rooting Algorithm with the value of *alpha* that maximizes the image quality enhancement measure (*GIQEM*).

We calculate *GIQEM* for every enhanced image: for enhanced image 1 (all image); for enhanced image 2 (blocks 8 by 8); for enhanced image 3 (blocks 16 by 16); and for enhanced image 4 (blocks 32 by 32).

Algorithm 4 Block-Rooting Method Using 3-D Block-Matching Scheme

Z is an original image.
1. Image splitting.
2. 3-D block-matching.
3. Enhancement processing.
4. The image quality enhancement measure calculation.
5. Weighted average.

$\tilde{Z}$ is the output of the enhanced image.

These values enable the calculation of weights as follows:

$$W_{\tilde{Z}_1} = M_{\tilde{Z}_1} \Big/ \sum\nolimits_i M_{\tilde{z}}(i), \quad W_{\tilde{Z}_8} = M_{\tilde{Z}_8} \Big/ \sum\nolimits_i M_{\tilde{z}}(i),$$
$$W_{\tilde{Z}_{16}} = M_{\tilde{Z}_{16}} \Big/ \sum\nolimits_i M_{\tilde{z}}(i), \quad W_{\tilde{Z}_{32}} = M_{\tilde{Z}_{32}} \Big/ \sum\nolimits_i M_{\tilde{z}}(i),$$

where M is the *GIQEM* for every block (for size = 8, 16, 32 and all image).

The resulting image is the weighted mean of all processing blocks:

$$\tilde{X} = \sum\nolimits_i M_{\tilde{z}}(i) \cdot W_{\tilde{z}}(i).$$

Adopted by [43] method, we can show that the time complexity of the proposed Algorithm is

$$\mathcal{O}(MNO_{I_{2D}}(N_1, N_1) + \mathcal{O}\left(MN \frac{\left(N_1^2 + N_2\right) N_S^2}{N_{step}^2}\right) + \mathcal{O}\left(MN \frac{\left(\mathcal{O}_{I_{3D}}(N_1, N_1, N_2)\right)}{N_{step}^2}\right) + \mathcal{O}\left(MNN_1 log_5 N_1\right)$$

where the first and the second term describe the block-matching procedure with Euclidean distance, the third term uses for denoising, and the fourth term uses for the image quality enhancement measure calculation; M and N are the numbers of the reference blocks in horizontal and vertical directions; $\mathcal{O}\mathfrak{F}_{2D}(N_1, N_1)$ and $\mathcal{O}\mathfrak{F}_{3D}(N_1, N_2, N_3)$ denote the complexity of the transforms $\mathfrak{F}_{2D}$ and $\mathfrak{F}_{3D}$; N_{step} is the step for reference blocks; N_1 is the size of the window of the weights; N_2 is the maximum number of the similar blocks to reference one; N_S is the size of the local neighborhood for searching candidate matching blocks. In this general form, time complexity mostly depends on the type of frequency transform.

IV. ENHANCEMENT QUALITY MEASURE

Estimation of the quality assessment after an enhancement process is a challenging problem. There is no universal measure that can specify both the enhancement method's objective and subjective validity [44]. There have been different

$$d(Z_{x_R}, Z_x) = \frac{\left\| \Upsilon'(\mathfrak{F}^{ht}_{2D}(Z_{x_R}), \lambda_{thr}\sqrt{2log(N_1^2)} - \Upsilon'(\mathfrak{F}^{ht}_{2D}(Z_x), \lambda_{thr}\sqrt{2log(N_1^2)} \right\|_2^2}{(N_1)^2},$$

definitions of performance based on contrast [10], [45] to find the optimum enhancement parameters. The block-rooting procedure depends on the parameter *alpha* (α). We are choosing the best (optimal) enhancement image through optimization of the proposed measure enhancement.

Both transform and spatial domain measures are primary groups of the human perception-based image enhancement quality measures. The spatial domain measures are calculated based on the pixel's values [46]. The AME and EME are examples of such spatial domain measures [47]. The transform domain measures based on DCT, DFT, or DWT [44]. In [48] authors proposed the contrast enhancement evaluation metrics based on the combined processing in the frequency and the spatial domains.

The second category of measure of image enhancement is the machine learning-based category [49].

The described non-reference image enhancement measures are summarized in Tables 1 and 2.

TABLE 1. Non-reference measure (Human perception-based).

NR measure	Definition
EME [44]	$EME_{k_1k_2} = \frac{1}{k_1k_2}\sum_{k=1}^{k_1}\sum_{l=1}^{k_2} 20\cdot \ln\left(\frac{I_{max,k,l}}{I_{min,k,l}}\right)$
EMEE [47]	$EMEE_{k_1k_2} = \frac{1}{k_1k_2}\sum_{k=1}^{k_1}\sum_{l=1}^{k_2} \alpha\left(\frac{I_{max,k,l}}{I_{min,k,l}}\right)^{\alpha}\cdot ln\left(\frac{I_{max,k,l}}{I_{min,k,l}}\right)$
Visibility [50]	$Visibility = \sum_{k=1}^{k_1}\sum_{l=1}^{k_2}\frac{I_{max,k,l}-I_{min,k,l}}{I_{max,k,l}+I_{min,k,l}}$
AME [10]	$AME_{k_1k_2} = -\frac{1}{k_1k_2}\sum_{k=1}^{k_1}\sum_{l=1}^{k_2} 20\cdot ln\left(\frac{I_{max,k,l}-I_{min,k,l}}{I_{max,k,l}+I_{min,k,l}}\right)$
SDME [50]	$SDME_{k_1k_2} = \frac{1}{k_1k_2}\sum_{k=1}^{k_1}\sum_{l=1}^{k_2} 20\cdot ln\left\|\frac{I_{max,k,l}-2I_{center,k,l}+I_{min,k,l}}{I_{max,k,l}+2I_{center,k,l}+I_{min,k,l}}\right\|$
TDME [47]	$TDME_k = \frac{\frac{1}{MN-k^2}\sum_{i=k}^{M}\sum_{j=k}^{N} Mag(DCT(i,j))}{\frac{1}{MN}\sum_{i=1}^{M}\sum_{j=1}^{N} Mag(DCT(i,j))}$

TABLE 2. Non-reference measure (*Machine learning-based*).

NR measure	Definition
BIQI [52]	*Machine learning-based approach (SVM)*
BLIINDS II [52]	*Machine learning-based approach (Probalistic model)*
BRISQUE [51]	*Natural scene statistic-based distortion-generic*
NIQE [53]	*Space domain natural scene statistic model*
IL-NIQE [53]	*Learning regression model*

As was shown in [46] for grayscale images, there is a direct correlation between the contrast enhancement of the image and the magnitude of high-frequency contents in the image's 2-D spectrum. In other words, if considering a block of k-by-k in the lower frequency section of the image, after contrast enhancement, some of the energy from this region will be transferred to the higher frequency region of the 2-D spectrum.

To launch a novel non-reference image assessment, we present a so-called Golden transform. The Golden Ratio has been used in many areas, such as art, design, mathematics, geometry, filtering, etc. [54].

It generated by using the Golden Ratio, which is created by the limit of the following sequence $x_n = F_{n+1}/F_n$, where F_n is the n-th Fibonacci number [55], [56], and where the Fibonacci Series defines as a sequence of numbers $F_n = F_{n-1} + F_{n-2}$, where $F_0 = 1$ and $F_n = 0$ for $n < 0$.

In this article, present the several properties of the Golden transform. The Golden transform 5×5 matrix G_5 is defined as [57]

$$\begin{bmatrix} 1 & 1 & 1 & 1 & 1 \\ 1 & \frac{1}{2\varphi}+j\frac{\varphi\gamma}{2} & -\frac{\varphi}{2}+j\frac{\gamma}{2} & -\frac{\varphi}{2}-j\frac{\gamma}{2} & \frac{1}{2\varphi}-j\frac{\varphi\gamma}{2} \\ 1 & -\frac{\varphi}{2}+j\frac{\gamma}{2} & \frac{1}{2\varphi}-j\frac{\varphi\gamma}{2} & \frac{1}{2\varphi}+j\frac{\varphi\gamma}{2} & -\frac{\varphi}{2}+j\frac{\gamma}{2} \\ 1 & -\frac{\varphi}{2}-j\frac{\gamma}{2} & \frac{1}{2\varphi}+j\frac{\varphi\gamma}{2} & \frac{1}{2\varphi}-j\frac{\varphi\gamma}{2} & -\frac{\varphi}{2}+j\frac{\gamma}{2} \\ 1 & \frac{1}{2\varphi}-j\frac{\varphi\gamma}{2} & -\frac{\varphi}{2}-j\frac{\gamma}{2} & -\frac{\varphi}{2}+j\frac{\gamma}{2} & \frac{1}{2\varphi}+j\frac{\varphi\gamma}{2} \end{bmatrix}$$

where

$$cos\frac{\pi}{2} = \frac{\varphi}{2}, sin\frac{\pi}{5} = \frac{\gamma}{2}a, \text{ and } \gamma = \sqrt{3-\varphi}.$$

Property 1: The 5×5 classical discrete Fourier transform is an approximation of Golden transforms [57]. The Fourier transform matrix is a complex-valued matrix defined as

$$\mathbf{W}_N = \begin{bmatrix} 1 & 1 & \cdots & 1 \\ 1 & \cos\left(2\Pi\frac{1}{N}\right) & \cdots & \cos\left(2\Pi\frac{N-1}{N}\right) \\ \vdots & \vdots & \ddots & \vdots \\ 1 & \cos\left(2\Pi\frac{N-1}{N}\right) & \cdots & \cos\left(2\Pi\frac{(N-1)^2}{N}\right) \end{bmatrix}$$

$$-j = \begin{bmatrix} 0 & 0 & \cdots & 0 \\ 0 & \sin\left(2\Pi\frac{1}{N}\right) & \cdots & \sin\left(2\Pi\frac{N-1}{N}\right) \\ 0 & \vdots & \ddots & \vdots \\ 0 & \sin\left(2\Pi\frac{N-1}{N}\right) & \cdots & \sin\left(2\Pi\frac{(N-1)^2}{N}\right) \end{bmatrix}$$

Property 2: The columns and rows of form Fibonacci Fourier transform matrix form the orthonormal vectors.

For every column and row, the condition for orthonormal vectors is satisfied, as

$$\sum\nolimits_i F5_{ij}\cdot F5_{ik} = \delta_{ij},$$
$$\sum\nolimits_i F5_{ji}\cdot F5_{ki} = \delta_{jk}.$$

where $i \in \{1, \ldots, n\}$, n is the matrix order, δ is the Kronecker symbol.

In other words, the scalar product of a row by itself is 1, and by any other row is 0. This is also true for columns.

Below we formulate the Golden transform domain-based image quality enhancement measure (*GIQEM*). The average magnitude of the Golden transform for the high-frequency region normalized by the average magnitude of coefficients for the entire image can be used to calculate the measure for the current sliding k_1-by-k_2 block. The core idea is that enhancing the contrast of an image creates more high-frequency content in the enhanced image. An increase in the magnitude of higher frequency coefficients suggests an enhancement in contrast in the image's luminance content [46].

Definition 3: Let's Z an image, k_1-by-k_2 block be a sliding block, to separate the regions of the image.

The Golden image quality enhancement measure (*GIQEM*) is defined as

$$GIQEM_{m_1m_2} = \frac{1}{k_1k_2} 20\, log \left(\frac{\sum \left|\tilde{Z}\right|}{\left|\tilde{Z}_{max}\right|} \right)$$

where $\tilde{Z}_{max}$ is the maximum magnitude in the frequency region for the current block and $\sum \left|\tilde{Z}\right|$ is the sum of magnitudes over the entire 2-D Golden transforms spectrum for the current block. We use the case where $k_1 = k_2 = 5$.

The overall *GIQEM* measure is the average of *GIQEM's* for each sliding *k*- by -*k* block:

$$GIQEM = \frac{1}{M_1M_2} \sum_{m_1=1}^{M_1} \sum_{m_2=1}^{M_2} GIQEM_{m_1m_2},$$

where M_1 and M_2 are amounts of the sliding *k-by-k* blocks by rows and columns respectively.

A fast Golden transforms algorithm with computational complexity $\mathcal{O}(Nlog_5N)$ can be designed.

V. OPTIMIZATION

The block-rooting transform depends on the parameter *alpha*. Figure 5 shows a comparative study of the enhanced images by the block-rooting method using different *alpha*.

We are choosing the best (optimal) enhancement image through optimization of the Golden image quality enhancement measure, so we select *alpha* in the proposed method for which *GIQEM* is maximum:

$$GIQEM(\Phi, \alpha_{opt}) = max \left\{ GIQEM(\Phi, \alpha) \right\}.$$

The main idea behind this measure is to use the relationship between the spread of the mean and the sum of the luminance values in the Fourier domain found in a small block. It then takes the average modulation in each block over the entire image.

Figure 6 shows the *GIQEM* dependence for different parameter alpha for the block-rooting method. When *alpha* equals to zero, only the phase is retained. In case $\alpha < 1$, the edges and details in the image are enhanced due to the magnitude of the large transform coefficients are reduced relative to the magnitude of the small coefficients. By varying the α -level and driving the edge information which depends on the high-frequency region, we are able to enhance

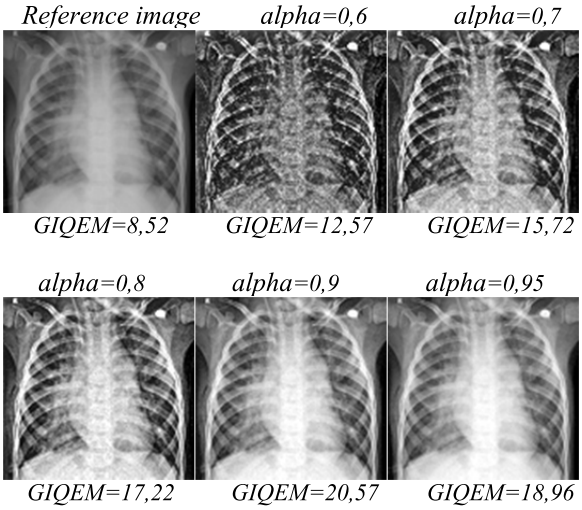

FIGURE 5. Proposed block-rooting transform with different *alpha*.

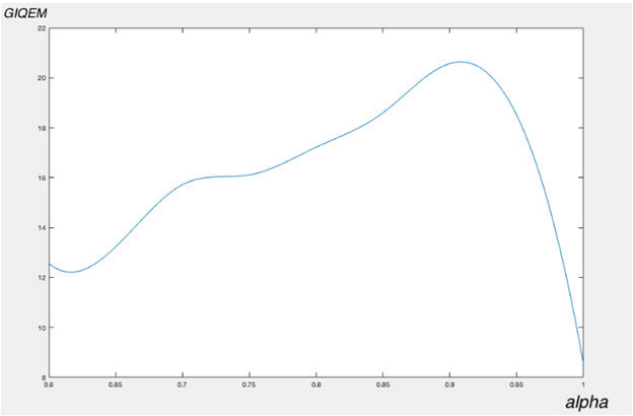

FIGURE 6. Plot of *GIQEM* vs *alpha* for block-rooting method.

the quality of images for the visualization. Figure 6 shows how to choose the best operator parameter *alpha* for the proposed block-rooting Algorithm. The optimal parameter $\alpha = 0,91$ for this test image. This case illustrates the process of enhancement, then the value *GIQEM* is maximum.

VI. EXPERIMENTAL RESULTS

A. GIQEM MEASURE EXPERIMENTAL RESULTS

We tested the proposed and the state-of-the-art quality measures on the dataset TID2008 [58], which allows estimating how a given metric corresponds to mean human perception. This dataset contains 25 reference images from Kodak Lossless True Color Image Suite and 1700 distorted images. In our experiment, we used only distortions with contrast change. The Mean Opinion Score (MOS, (0 -minimal, 9 - maximal) was obtained from the results of 838 experiments carried out by observers.

We calculate the Pearson correlation coefficient (*PCC)* as:

$$PCC = \frac{\mathbb{E}\left[(X - \mu_X)(Y - \mu_Y)\right]}{\sigma_X \sigma_Y},$$

where μ_X and μ_Y are the mean values, σ_X and σ_Y are the standard deviations, and E is the expectation.

And the standard deviation (SD) for all received coefficient correlation by:

$$SD = \sqrt{\frac{1}{N-1}} \sum_{i=1}^{N} (x_i - \mu_x),$$

where x_i are the observed values of the sample items, μ_x is the mean value of these observations, and N is the number of observations in the sample.

To assess the effectiveness of the proposed metric of the visual quality of images, a comparison is made between Pearson's coefficient correlation and standard deviation based on test images of TID2008. The average results for all test images are given in Table 3. We also compare the proposed metric with other non-reference metrics *(AME, EMEE, SDME, Visibility, TDME, BIQI, BRISQUE, ILNIQE, NIQE).*

TABLE 3. Non-reference measures.

NR measures	*PCC*	*SD*
EME	*0,803*	*0,103*
AME	*0,918*	*0,207*
EMEE	*0,685*	*0,138*
SDME	*0,900*	*0,249*
Visibility	*0,926*	*0,072*
TDME	*0,898*	*0,101*
BIQI	*0,412*	*0,113*
BRISQUE	*0,041*	*0,301*
ILNIQE	*0,014*	*0,285*
NIQE	*0,018*	*0,209*
GIQEM (proposed)	***0,935***	***0,048***

The accuracy of the proposed metric estimated by the Pearson correlation coefficient (PCC) and the SD shows the monotonicity of the prediction image quality with mean opinion score (MOS). Correlation values closer to $+1$ indicate agreement between the MOS, and the measure and closer to -1 indicate complete disagreement. A correlation value shows how our proposed measure agrees with human visual perception. The proposed measure *GIQEM* provides an accurate interpretation of the image quality with comparison to human visual perception. Figure 7 shows the medical images with different levels of the same distortion type and corresponding non-reference metrics.

In these images, improved perception is difficult to qualify. All non-reference metrics show different results. There is no universal measure that can specify both the objective and subjective validity of the enhanced images. A number of images, which clearly illustrated an improved contrast, showed no consistency, as a class, when using these statistical-based metrics.

The *GIQEM* shows the best result for image #2 (the first row), but visually, this image has low contrast. This error can be explained by the fact that the proposed quality measure is based on an assessment of the ratio of the spectral components; respectively, the best results will be for images with

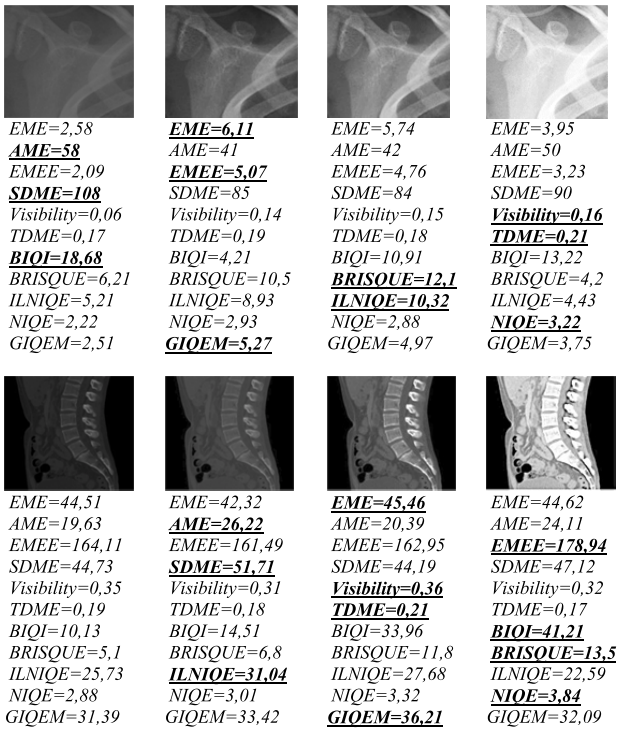

FIGURE 7. Golden transform and other metrics for original and enhanced images.

a large number of details and boundaries. For the second row, the proposed metric shows the highest value for image #3, which is also consistent with visual analysis.

The *GIQEM* measure of image quality operates in the Discrete Fourier Transform domain and proposed Fibonacci Fourier transform. Since most imaging acquisition systems operate in the spectral domain for image compression, the transform operation is often built-in in the hardware processors, making it appealing for real-time applications. Besides, many of the image enhancement algorithms operate in the DCT domain as well, meaning that our proposed measure eliminates the need for conversion between the spatial and transform domain for image evaluation, hence accelerating the enhancement process.

B. BLOCK-ROOTING METHOD EXPERIMENTAL RESULTS

To provide a comparison of the proposed enhancement algorithm, three publicly available databases are used: 1) ChestX-ray, 2) fastMRI, and 3) NYU (Fig. 8). As an example, Table 4 lists publicly available CT and MR datasets containing raw k-space data.

ChestX-ray [59] is a large dataset of chest x-rays and competition for automated chest x-ray interpretation. The dataset contains over 108,948 frontal view x-ray images of 32,717 unique patients.

FastMRI [60] is an anonymized imaging dataset that comprises raw k-space data from more than 6,970 fully sampled brain MRIs and DICOM images from 10,000 clinical brain MRIs.

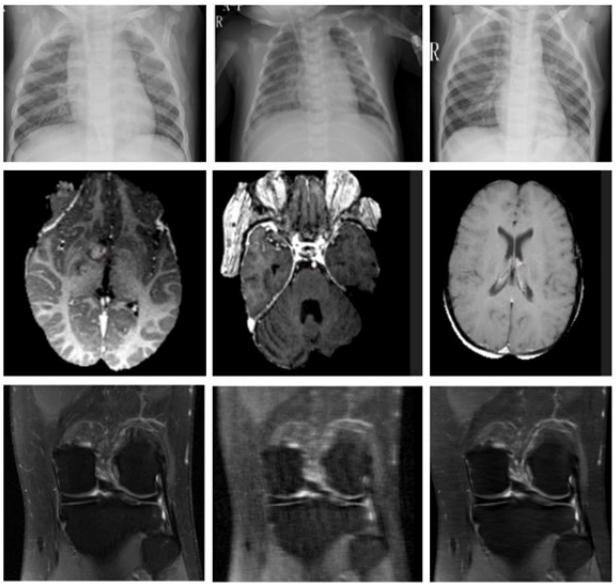

FIGURE 8. Examples from the datasets.

TABLE 4. Publicly available MRI and CT datasets.

Dataset	Volumes	Body part
ChestX-ray dataset [59]	*108,948*	*chest*
fastMRI dataset [60]	*6,970*	*brain*
NYU dataset [61]	*100*	*knee*

NYU dataset [61] is an open science neuroinformatic database storing datasets from human imaging research studies.

Figure 9 demonstrates the image-enhancement results using the proposed Algorithm for different medical-image data sets. The enhanced results of the proposed method look clear and global, and the local contrast is well enhanced. In order to improve our images, we reduce the magnitude information of each image while leaving the phase information intact [44]. Since the phase information is much more significant than the magnitude information in the determination of edges, reducing the magnitude produces better edge detection capabilities [44].

In our experiments, the results are compared with those of other global and block-based well-designed contrast enhancement methods: the contrast-limited adaptive histogram equalization algorithm (CLAHE), the Low-light image enhancement (LIME) [62], the Robust Retinex [63], the Multi-scale Retinex (MSRCR) [64], the Contrast enhancement using exposure fusion (CAIP) [65], and the Joint enhancement via sequential decomposition (JED) [66]. Figures 10-11 demonstrate the image enhancement results and some zoomed parts obtained by various algorithms, respectively: a) the original image; b) the enhanced image by the CLAHE; c) the enhanced image by the LIME; d) the enhanced image by the Robust Retinex; e) the enhanced image by the MSRCR; f) the enhanced image by the CAIP; g) the enhanced image by the JED; and h) the enhanced image by the proposed method.

TABLE 5. Non-reference measures for NYU dataset.

	Original	*CLAHE*	*LIME*	*Robust Retinex*	*MSRCR*	*CAIP*	*JED*	*Proposed method*
EME	*36,12*	*37,88*	*31,13*	*30,97*	*10,29*	*33,33*	*28,09*	***43,85***
AME	*16,47*	*12,44*	*14,85*	*17,42*	*16,34*	*13,76*	*17,85*	***18,59***
EMEE	*29,31*	*47,64*	*32,54*	*72,67*	*25,25*	*66,56*	*69,23*	***80,93***
SDME	*47,11*	*55,04*	*54,89*	*73,84*	*68,81*	***79,37***	*74,97*	*61,25*
Visibility	*0,55*	*0,61*	*0,25*	*0,26*	*0,14*	*0,27*	*0,22*	***0,62***
TDME	*0,18*	***0,22***	*0,17*	*0,11*	*0,15*	*0,09*	*0,11*	*0,15*
BIQI	*56,83*	***69,23***	*63,54*	*41,21*	*42,82*	*51,55*	*51,22*	*59,76*
BRISQUE	*5,43*	*8,41*	*10,51*	***13,12***	*12,12*	*7,58*	*9,32*	*9,67*
ILNIQE	*8,98*	*18,78*	*16,78*	*10,31*	*19,34*	*11,23*	*18,98*	***22,45***
NIQE	*2,88*	*3,06*	*3,11*	*3,13*	*2,56*	*2,97*	*3,12*	***3,22***
GIQEM	*8,71*	*15,63*	*16,38*	*18,21*	*7,82*	*18,23*	*17,85*	***18,66***

TABLE 6. Non-reference measures for FastMRI dataset.

	Original	*CLAHE*	*LIME*	*Robust Retinex*	*MSRCR*	*CAIP*	*JED*	*Proposed method*
EME	*31,22*	*28,77*	*25,03*	*26,62*	*23,95*	*26,03*	*28,82*	***44,38***
AME	*15,67*	*12,21*	*14,59*	*15,76*	*10,11*	*17,65*	*18,78*	***20,33***
EMEE	*21,77*	*27,57*	*30,61*	*12,55*	*11,66*	*21,87*	*25,27*	***46,12***
SDME	*53,74*	*61,79*	*56,85*	*59,76*	*51,23*	*57,23*	*53,78*	***62,91***
Visibility	*0,51*	*0,56*	*0,21*	*0,12*	*0,12*	*0,14*	*0,11*	***0,61***
TDME	*0,19*	*0,22*	*0,14*	*0,09*	*0,11*	*0,09*	*0,08*	***0,31***
BIQI	*23,92*	*47,48*	***51,19***	*23,56*	*28,52*	*30,58*	*30,05*	*47,82*
BRISQUE	*4,91*	***13,58***	*5,65*	*8,21*	*6,34*	*7,52*	*10,34*	*11,53*
ILNIQE	*4,68*	*8,12*	*7,21*	*8,32*	*6,56*	*9,23*	*13,78*	***14,23***
NIQE	*2,31*	*2,54*	*2,34*	*2,23*	*2,34*	*2,44*	*2,51*	***2,59***
GIQEM	*7,22*	*12,01*	*6,19*	*8,78*	*3,54*	*7,42*	*8,58*	***14,23***

TABLE 7. Non-reference measures for ChestX-ray Dataset.

	Original	*CLAHE*	*LIME*	*Robust Retinex*	*MSRCR*	*CAIP*	*JED*	*Proposed method*
EME	*17,18*	*19,23*	*21,08*	*12,39*	*27,62*	*21,43*	*21,89*	***31,88***
AME	*12,23*	*15,22*	*13,07*	*11,06*	*17,42*	*16,98*	*17,23*	***20,78***
EMEE	*35,88*	*41,21*	*34,45*	*32,72*	*38,53*	*27,78*	*42,21*	***46,12***
SDME	*57,51*	*67,98*	*66,89*	*68,34*	*66,22*	*68,44*	*57,98*	***71,52***
Visibility	*0,28*	*0,32*	*0,11*	*0,19*	*0,16*	*0,04*	*0,03*	***0,54***
TDME	*0,16*	*0,23*	*0,14*	*0,13*	*0,14*	*0,12*	*0,13*	***0,26***
BIQI	*36,12*	*40,75*	*16,81*	*13,04*	*18,82*	*12,11*	*17,78*	***55,88***
BRISQUE	*5,57*	***14,16***	*9,34*	*4,21*	*12,32*	*8,78*	*11,87*	*14,11*
ILNIQE	*10,21*	*21,76*	*14,34*	*9,21*	*19,34*	*12,56*	*17,34*	***25,23***
NIQE	*2,34*	***2,87***	*2,38*	*2,22*	*2,65*	*2,33*	*2,45*	*2,78*
GIQEM	*5,51*	*7,86*	*3,63*	*3,15*	*7,25*	*4,33*	*6,21*	***10,15***

The experimental results for the image ≪Brain≫ from fastMRI dataset are given in Figure 10. When determining the enhanced result, we should make a compromise between noise suppression and tiny detail preservation. For the local CLAHE method, some artifacts appear in the enhanced result. As the block size increases to all images, the local contrast enhancement is not as good as that obtained by small

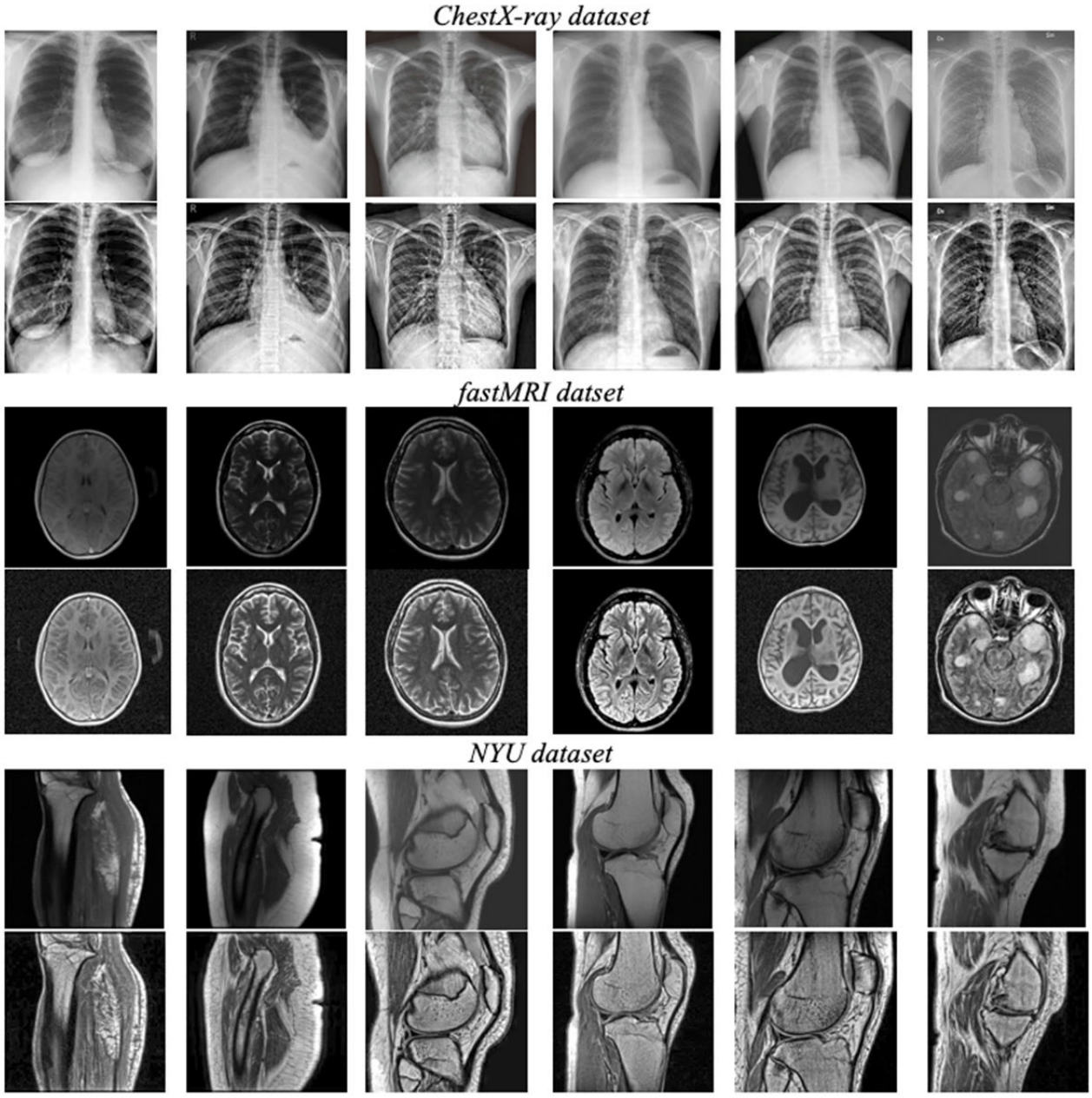

FIGURE 9. Examples of image enhancement.

block size, but this contrast enhancement reduction is not obvious. The enhanced result of CLAHE looks unnatural due to the appearance of block artifacts. The original image ≪Brain≫ is slightly dark, and this dark tone disappears after applying the Robust Retinex and JED algorithms. The images (Fig. 10c and 10e) after processing by the LIME and MSRCR methods have low contrast and low visibility. On the other hand, the result of applying CAIP saturates the colors excessively (Fig. 10f).

Our experiments for the proposed method set the block sizes to 8 by 8, 16 by 16, 32 by 32 and 64 by 64. The proposed approach could have the ability to boost the contrast in digital images in an efficient manner. The fuzzy procedure reduces the noise, efficiently preserves the edges, and provides visually pleasant results. Additionally, the proposed technique uses illuminate normalization to reduce illuminated artifacts.

The experimental results for the image ≪Knee≫ from the NYU dataset are given in Figure 11. In CLAHE, the clip factor is set as $\alpha = 0.01$, and the block size set to be 64×64. For good enhancement results, they should obtain better local contrast enhancement and noise suppression, be artifact-free, and visually pleasing. The image after CLAHE processing is oversaturated, the areas become too bright and too dark, and

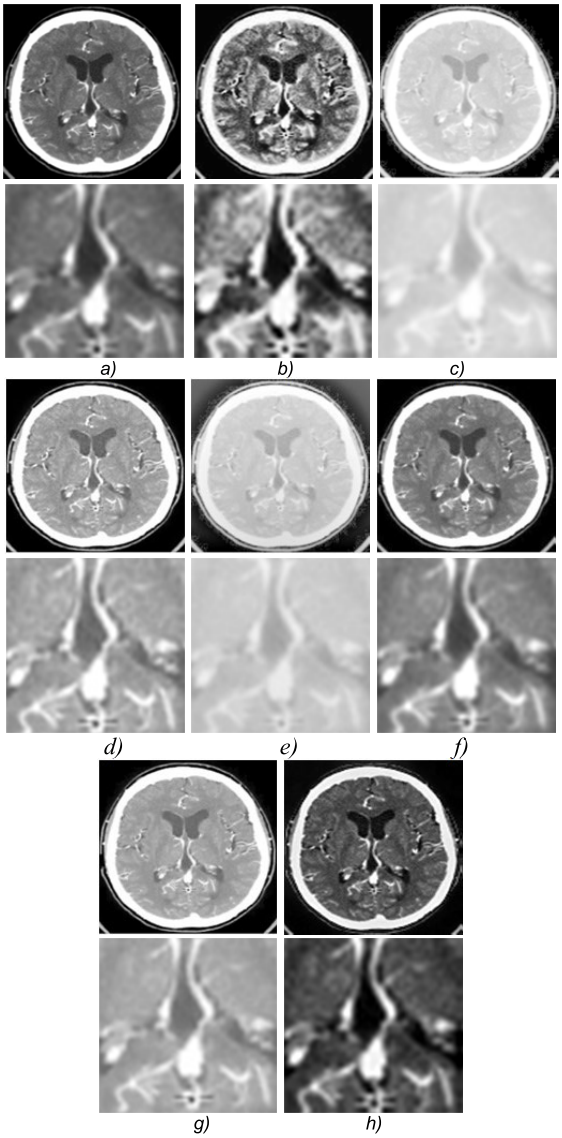

FIGURE 10. Examples of image enhancement ≪Brain≫.

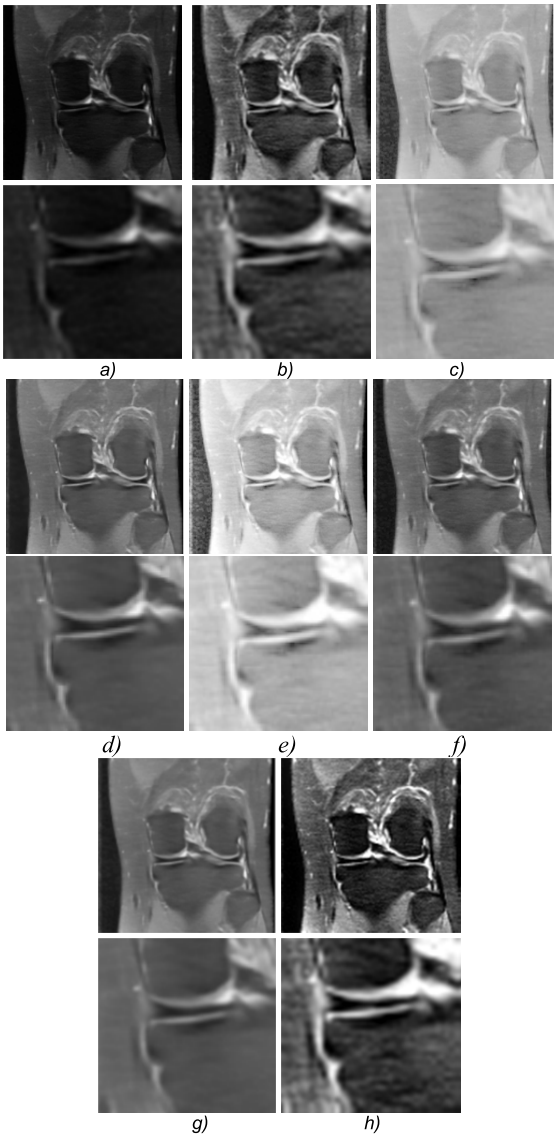

FIGURE 11. Examples of image enhancement ≪Knee≫.

some image details are disappeared, e.g., the edge of the down part of the knee is covered by background.

The CAIP method over-enhance the test image in bright regions. The enhanced results of CLAHE and the proposed method appear similar with respect to the bone image. The MSRCR and LIME causes noise amplification in the image, which greatly reduces its performance compared with the other methods. The partial boundary of the bones disappears in the Robust Retinex and the JED result, and some details in the CLAHE result were also lost. In Figure 11, due to the existence of nonuniformity, the enhanced result of CLAHE looks poor because it is sensitive to the nonuniformity. The proposed method saves some details near the border of objects. This is caused by the correct classification using different block sizes in the transition region between the detail region and homogeneous region. It is clear that the proposed method gets better local and global contrast enhancement than other methods.

In Figure 12, the results for the image ≪Chest≫ from the ChestX-ray dataset are given obtained by various algorithms, respectively: a) the original image; b) the enhanced image by the CLAHE; c) the enhanced image by the MSRCR; and d) the enhanced image by the proposed method. The details of the chest in the result using the proposed method look clearer than those in the CLAHE and MSRCR results. Some parts of the chest in the left down region in the enhanced result of CLAHE cannot be distinguished from the background. The local contrast enhancement of the MSRCR result is not as good as those of the other methods. In the enhanced result of CLAHE, many details of the image are smoothed.

Once again, CLAHE does not produce better local contrast enhancement, and the proposed method outperforms the other methods with no artifacts, good appearance, and fine details.

The block-rooting approach produces a better-enhanced result with a natural appearance and non-uniformity

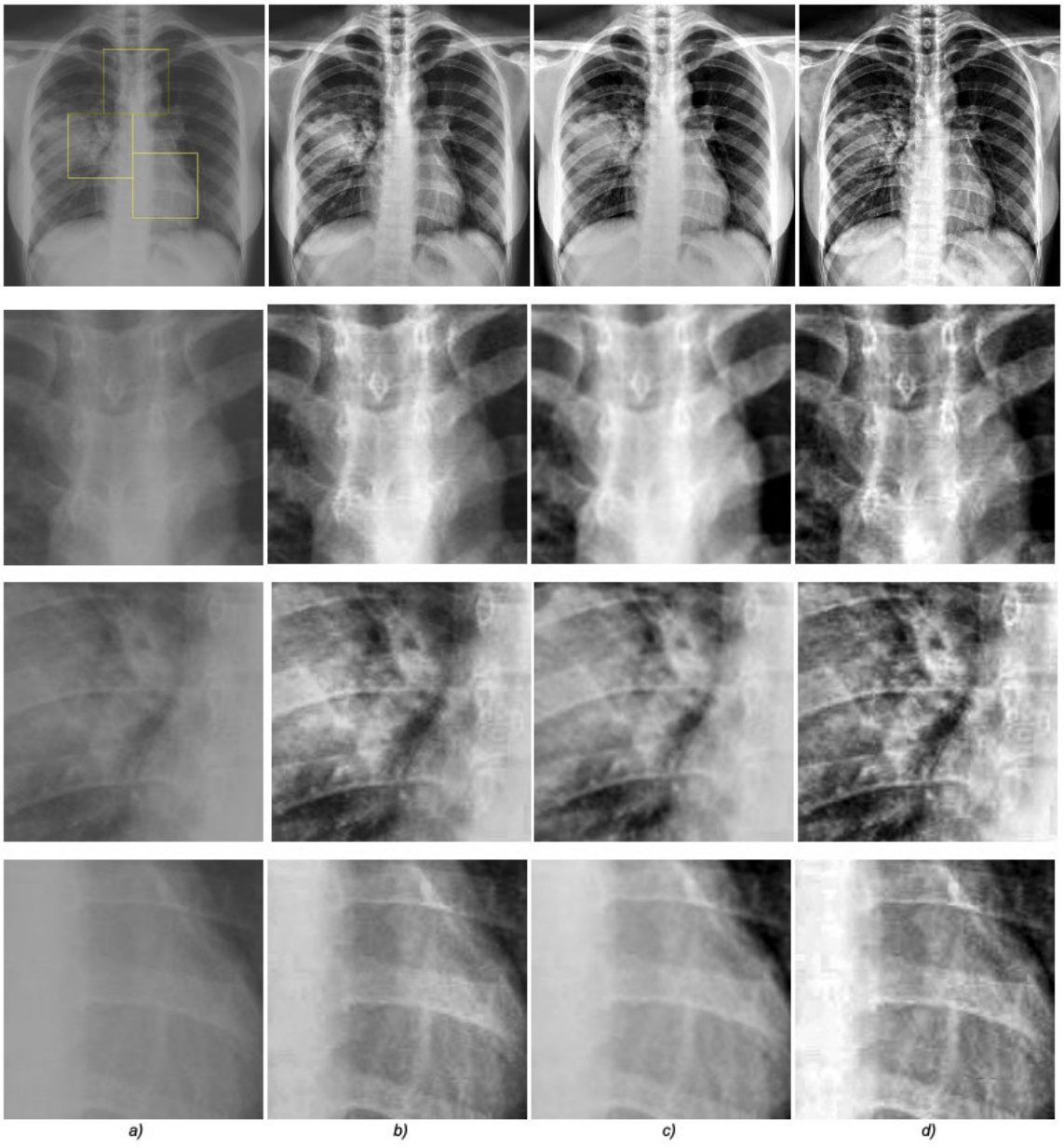

FIGURE 12. Examples of image enhancement ≪Chest≫.

suppression. The proposed method is proven to be the best method than CLAHE and MSRCR, because it can significantly increase the contrast and remove the noise. Tables 5–7 give comparative results of the non-reference enhancement measures for test datasets by the seven methods. The better results for every measure are marked in bold in the tables. The experimental results show that the enhancement images by the proposed method have the highest *GIQEM*.

The proposed method provides almost the highest *EME*, *AME, EMEE, TDME, Visibility,* and *ILNIQE* values, except *BIQI, SDME* and *BRISQUE* for NYU, and fastMRI datasets. The values of the metrics demonstrate that the proposed method outperforms the other methods in terms of local contrast enhancement and performs well on the structural similarity, detail improvement, and naturalness preservation.

Extensive computer simulations show that the presented approach demonstrates that it overperforms state-of-the-art methods (such as CLAHE, Retinex, MSRCR, CAIP, JED, and LIME), and it is suitable for real-time processing of low contrast images. The results show strong correlations between the presented measures and mean opinion score.

VII. CONCLUSION

We present a novel image enhancement algorithm based on combined local and global image processing. The basic idea is to apply a 3-D block-rooting scheme for blocks on the

image with different sizes. To optimize the block rooting procedure, we proposed a novel image enhancement measure in the Golden transform (frequency) domain. The suggested image enhancement results compare favorably against other state-of-the-art approaches. The extensive computer simulations demonstrate that the proposed system achieves good performances and can prevent noise increasing during the sharpening of the image details.

A limitation of the proposed approach is that the large uniform regions include some noise after enhancement. Although the proposed approach reduces this effect significantly compared to the traditional domain-based methods with high-frequency enhancement, this effect is not entirely suppressed, which can be a point of interest for further research.

REFERENCES

[1] V. Voronin, E. Semenishchev, M. Ponomarenko, and S. Agaian, "Combined local and global image enhancement algorithm," in *Proc. 16th Electron. Imag., Image Process., Algorithms Syst.*, 2019, pp. 1–5.

[2] W. Yong, L. Ting, and Q. Yongsheng, "Image enhancement algorithm research based on the archives monitoring under low illumination," in *Proc. 12th IEEE Int. Conf. Electron. Meas. Instrum. (ICEMI)*, Jul. 2015, pp. 1270–1274.

[3] D. A. Lavigne, M. Breton, M. Pichette, V. Larochelle, and J.-R. Simard, "Enhanced military target discrimination using active and passive polarimetric imagery," in *Proc. IEEE Int. Geosci. Remote Sens. Symp. (IGARSS)*, 2008, pp. V-354–V-357.

[4] V. Voronin, A. Zelensky, and S. Agaian, "Feedback Alfa-rooting algorithm for medical image enhancement," in *Proc. 18th Electron. Imag., Image Process., Algorithms Syst.*, 2019, pp. 223-1–223-6.

[5] L. Hong, Y. Wan, and A. Jain, "Fingerprint image enhancement: Algorithm and performance evaluation," *IEEE Trans. Pattern Anal. Mach. Intell.*, vol. 20, no. 8, pp. 777–789, Aug. 1998, 10.1109/34.709565.

[6] S.-C. Huang, B.-H. Chen, and Y.-J. Cheng, "An efficient visibility enhancement algorithm for road scenes captured by intelligent transportation systems," *IEEE Trans. Intell. Transp. Syst.*, vol. 15, no. 5, pp. 2321–2332, Oct. 2014.

[7] C. Li, J. Liu, A. Liu, Q. Wu, and L. Bi, "Global and adaptive contrast enhancement for low illumination gray images," *IEEE Access*, vol. 7, pp. 163395–163411, 2019.

[8] A. Grigoryan and S. Agaian, "Image enhancement," in *Advances in Imaging and Electron Physics*. New York, NY, USA: Academic, 2004, pp. 165–243.

[9] X. Qiao, J. Bao, H. Zhang, L. Zeng, and D. Li, "Underwater image quality enhancement of sea cucumbers based on improved histogram equalization and wavelet transform," *Inf. Process. Agricult.*, vol. 4, no. 3, pp. 206–213, Sep. 2017.

[10] S. S. Agaian, B. Silver, and K. A. Panetta, "Transform coefficient histogram-based image enhancement algorithms using contrast entropy," *IEEE Trans. Image Process.*, vol. 16, no. 3, pp. 741–758, Mar. 2007.

[11] S. S. Agaian, K. Panetta, and A. M. Grigoryan, "Transform-based image enhancement algorithms with performance measure," *IEEE Trans. Image Process.*, vol. 10, no. 3, pp. 367–382, Mar. 2001.

[12] J. S. Duncan and N. Ayache, "Medical image analysis: Progress over two decades and the challenges ahead," *IEEE Trans. Pattern Anal. Mach. Intell.*, vol. 22, no. 1, pp. 85–106, Jan. 2000.

[13] S. Fu, M. Zhang, C. Mu, and X. Shen, "Advancements of medical image enhancement in healthcare applications," *J. Healthcare Eng.*, vol. 2018, pp. 1–2, Mar. 2018.

[14] S. M. Pizer, E. P. Amburn, J. D. Austin, R. Cromartie, A. Geselowitz, T. Greer, B. H. Romeny, J. B. Zimmerman, and K. Zuiderveld, "Adaptive histogram equalization and its variations," *Comput. Vis., Graph., Image Process.*, vol. 39, no. 3, pp. 355–368, 1987.

[15] J. A. Stark, "Adaptive image contrast enhancement using generalizations of histogram equalization," *IEEE Trans. Image Process.*, vol. 9, no. 5, pp. 889–896, May 2000.

[16] K. Zuiderveld, "Contrast limited adaptive histogram equalization," in *Graphics Gems IV*, P. Heckbert, Ed. New York, NY, USA: Academic, 1994.

[17] R. H. Sherrier and G. A. Johnson, "Regionally adaptive histogram equalization of the chest," *IEEE Trans. Med. Imag.*, vol. 6, no. 1, pp. 1–7, Mar. 1987.

[18] P. M. Narendra and R. C. Fitch, "Real-time adaptive contrast enhancement," *IEEE Trans. Pattern Anal. Mach. Intell.*, vol. PAMI-3, no. 6, pp. 655–661, Nov. 1981.

[19] S. M. Pizer, E. P. Amburn, J. D. Austin, R. Cromartie, A. Geselowitz, T. Greer, B. H. Romeny, J. B. Zimmerman, and K. Zui derveld, "Adaptive histogram equalization and its variations," *Comput. Vis. Graph. Image Process.*, vol. 39, no. 3, pp. 355–368, Sep. 1987, doi: 10.1016/S0734-189X(87)80186-X.

[20] Y. Wang, W. Song, G. Fortino, L.-Z. Qi, W. Zhang, and A. Liotta, "An experimental-based review of image enhancement and image restoration methods for underwater imaging," *IEEE Access*, vol. 7, pp. 140233–140251, 2019.

[21] P. N. Puiono, I. K. E. Purnama, and M. Hariadi, "Color enhancement of underwater voral reef images using contrast limited adaptive histogram equalization (CLAHE) with Rayleigh distribution," in *Proc. 7th ICTS*, Bali, Indonesia, 2013, pp. 14233–140251.

[22] K. Liang, Y. Ma, Y. Xie, B. Zhou, and R. Wang, "A new adaptive contrast enhancement algorithm for infrared images based on double plateaus histogram equalization," *Infr. Phys. Technol.*, vol. 55, no. 4, pp. 309–315, Jul. 2012.

[23] Y.-T. Kim, "Contrast enhancement using brightness preserving bi-histogram equalization," *IEEE Trans. Consum. Electron.*, vol. 43, no. 1, pp. 1–8, 1997.

[24] S.-C. Huang, F.-C. Cheng, and Y.-S. Chiu, "Efficient contrast enhancement using adaptive gamma correction with weighting distribution," *IEEE Trans. Image Process.*, vol. 22, no. 3, pp. 1032–1041, Mar. 2013.

[25] K. Gu, G. Zhai, W. Lin, and M. Liu, "The analysis of image contrast: From quality assessment to automatic enhancement," *IEEE Trans. Cybern.*, vol. 46, no. 1, pp. 284–297, Jan. 2016.

[26] K. Gu, D. Tao, J.-F. Qiao, and W. Lin, "Learning a no-reference quality assessment model of enhanced images with big data," *IEEE Trans. Neural Netw. Learn. Syst.*, vol. 29, no. 4, pp. 1301–1313, Apr. 2018.

[27] K. Gu, G. Zhai, X. Yang, W. Zhang, and C. Wen Chen, "Automatic contrast enhancement technology with saliency preservation," *IEEE Trans. Circuits Syst. Video Technol.*, vol. 25, no. 9, pp. 1480–1494, Sep. 2015.

[28] S.-C. Huang, F.-C. Cheng, and Y.-S. Chiu, "Efficient contrast enhancement using adaptive gamma correction with weighting distribution," *IEEE Trans. Image Process.*, vol. 22, no. 3, pp. 1032–1041, Mar. 2013.

[29] R. T. Hamid, "Fuzzy image enhancement: An overview," in *Fuzzy Techniques in Image Processing*. Berlin, Germany: Springer-Verlag, 2000, pp. 137–171.

[30] M. Hanmandlu and D. Jha, "An optimal fuzzy system for color image enhancement," *IEEE Trans. Image Process.*, vol. 15, no. 10, pp. 2956–2966, Oct. 2006.

[31] J. Zhang, G. Yang, Q. Xu, and Y. Zhao, "Adaptive calculation of division points for piecewise linear transformation and application in image enhancement," in *Proc. Int. Conf. Environ. Sci. Inf. Appl. Technol.*, Jul. 2009, pp. 645–648.

[32] A. M. Nickfarjam and H. Ebrahimpour-Komleh, "Multi-resolution gray-level image enhancement using particle swarm optimization," *Int. J. Speech Technol.*, vol. 47, no. 4, pp. 1132–1143, Dec. 2017.

[33] M. K. Osman, M. Y. Mashor, Z. Saad, and H. Jaafar, "Contrast enhancement for ziehl-neelsen tissue slide images using linear stretching and histogram equalization technique," in *Proc. IEEE Symp. Ind. Electron. Appl.*, Oct. 2009, pp. 431–435.

[34] T. S. Sazzad, M. Z. Hasan, F. Mohammed, and S. Islam, "Gamma encoding on image processing considering human visualization, analysis and comparison," *Int. J. Comput. Sci. Eng.*, vol. 4, no. 12, p. 1868, 2012.

[35] J.-M. Morel, A. B. Petro, and C. Sbert, "Fast implementation of color constancy algorithms," *Proc. SPIE*, vol. 7244, Jan. 2009, Art. no. 724106.

[36] R. Kimmel, M. Elad, D. Shaked, R. Keshet, and I. Sobel, "A variational framework for Retinex," *Int. J. Comput. Vis.*, vol. 52, no. 1, pp. 7–23, 2003.

[37] W. Wang, B. Li, J. Zheng, S. Xian, and J. Wang, "A fast multi-scale retinex algorithm for color image enhancement," in *Proc. Int. Conf. Wavelet Anal. Pattern Recognit.*, Aug. 2008, pp. 80–85.

[38] D. J. Jobson, Z. Rahman, and G. A. Woodell, "A multiscale retinex for bridging the gap between color images and the human observation of scenes," *IEEE Trans. Image Process.*, vol. 6, no. 7, pp. 965–976, Jul. 1997.

[39] S. Agaian and F. Arslan, "Two transform based image enhancement methods," in *Proc. Int. Signal Process. Conf.*, Dallas, TX, USA, 2003, pp. 125–136.

[40] V. Voronin, E. Semenishchev, A. Zelensky, and S. Agaian, "Quaternion-based local and global color image enhancement algorithm," *Proc. SPIE*, vol. 10993, May 2019, Art. no. 1099304.
[41] J. Mukherjee and S. K. Mitra, "Enhancement of color images by scaling the DCT coefficients," *IEEE Trans. Image Process.*, vol. 17, no. 10, pp. 1783–1794, Oct. 2008.
[42] J. Cepeda-Negrete, R. E. Sanchez-Yanez, F. E. Correa-Tome, and R. A. Lizarraga-Morales, "Dark image enhancement using perceptual color transfer," *IEEE Access*, vol. 6, pp. 14935–14945, 2018.
[43] K. Dabov, A. Foi, V. Katkovnik, and K. Egiazarian, "Image denoising by sparse 3-D transform-domain collaborative filtering," *IEEE Trans. Image Process.*, vol. 16, no. 8, pp. 2080–2095, Aug. 2007.
[44] S. S. Agaian, K. Panetta, and A. M. Grigoryan, "Transform-based image enhancement algorithms with performance measure," *IEEE Trans. Image Process.*, vol. 10, no. 3, pp. 367–382, Mar. 2001.
[45] A. Beghdadi and A. Le Negrate, "Contrast enhancement technique based on local detection of edges," *Comput. Vis. Graph. Image Process.*, vol. 46, pp. 162–274, May 1989.
[46] A. Samani, K. Panetta, and S. Agaian, "Transform domain measure of enhancement—TDME–for security imaging applications," in *Proc. IEEE Int. Conf. Technol. Homeland Secur. (HST)*, 2013, pp. 265–270.
[47] K. Panetta, E. J. Wharton, and S. Agaian, "Human visual system-based image enhancement and logarithmic contrast measure," *IEEE Trans. Syst. Man Cybern., B, Cybern.*, vol. 38, no. 1, pp. 174–188, Jan. 2008.
[48] M. A. Qureshi, A. Beghdadi, and M. Deriche, "Towards the design of a consistent image contrast enhancement evaluation measure," *Signal Process., Image Commun.*, vol. 58, pp. 212–227, Oct. 2017.
[49] J. Tang, E. Peli, and S. Acton, "Image enhancement using a contrast measure in the compressed domain," *IEEE Signal Process. Lett.*, vol. 10, no. 10, pp. 289–292, Oct. 2003.
[50] C. Gao, K. Panetta, and S. Agaian, "No reference color image quality measures," in *Proc. IEEE Int. Conf. Cybern. (CYBCO)*, Jun. 2013, pp. 243–248.
[51] A. Mittal, R. Soundararajan, and A. C. Bovik, "Making a 'Completely blind' image quality analyzer," *IEEE Signal Process. Lett.*, vol. 20, no. 3, pp. 209–212, Mar. 2013.
[52] A. Mittal, A. K. Moorthy, and A. C. Bovik, "No-reference image quality assessment in the spatial domain," *IEEE Trans. Image Process.*, vol. 21, no. 12, pp. 4695–4708, Dec. 2012.
[53] L. Zhang, L. Zhang, and A. C. Bovik, "A feature-enriched completely blind image quality evaluator," *IEEE Trans. Image Process.*, vol. 24, no. 8, pp. 2579–2591, Aug. 2015.
[54] D. R. Mack, "The magical fibonacci number," *IEEE Potentials*, vol. 9, no. 3, pp. 34–35, Oct. 1990.
[55] S. Agaian, J. Astola, K. Egiazarian, and P. Kuosmanen, "Decompositional methods for stack filtering using Fibonacci p-codes," *Signal Process.*, vol. 41, pp. 101–110, Jan. 1995.
[56] D. Z. Gevorkian, K. O. Egiazarian, S. S. Agaian, J. T. Astola, and O. Vainio, "Parallel algorithms and VLSI architectures for stack filtering using fibonacci p-codes," *IEEE Trans. Signal Process.*, vol. 43, no. 1, pp. 286–295, 1995.
[57] S. S. Agaian, C. L. P. Chen, and M.-C. Chen, "Fibonacci Fourier transform and sliding window filtering," in *Proc. IEEE Int. Conf. Syst. Syst. Eng.*, Apr. 2007, pp. 1–5.
[58] N. Ponomarenko, V. Lukin, A. Zelensky, K. Egiazarian, M. Carli, and F. Battisti, "TID2008—A database for evaluation of full-reference visual quality assessment metrics," *Adv. Mod. Radioelectron.*, vol. 10, no. 4, pp. 30–45, 2009.
[59] X. Wang, Y. Peng, L. Lu, Z. Lu, M. Bagheri, and R. M. Summers, "ChestX-ray8: hospital-scale chest X-ray database and benchmarks on weakly-supervised classification and localization of common thorax diseases," in *Proc. IEEE Conf. Comput. Vis. Pattern Recognit. (CVPR)*, Jul. 2017, pp. 3462–3471.
[60] J. Zbontar *et al.*, "FastMRI: An open dataset and benchmarks for accelerated MRI," 2018, *arXiv:1811.08839*. [Online]. Available: http://arxiv.org/abs/1811.08839
[61] K. Hammernik, T. Klatzer, E. Kobler, M. P. Recht, D. K. Sodickson, T. Pock, and F. Knoll, "Learning a variational network for reconstruction of accelerated MRI data," *Magn. Resonance Med.*, vol. 79, no. 6, pp. 3055–3071, 2018.
[62] X. Guo, "LIME: A method for low-light IMage enhancement," in *Proc. 24th ACM Int. Conf. Multimedia*, Oct. 2016, pp. 87–91.
[63] M. Li, J. Liu, W. Yang, X. Sun, and Z. Guo, "Structure-revealing low-light image enhancement via robust retinex model," *IEEE Trans. Image Process.*, vol. 27, no. 6, pp. 2828–2841, Jun. 2018.
[64] J. Ma, X. Fan, J. Ni, X. Zhu, and C. Xiong, "Multi-scale Retinex with color restoration image enhancement based on Gaussian filtering and guided filtering," *Int. J. Mod. Phys. B*, vol. 31, nos. 16–19, Jul. 2017, Art. no. 1744077.
[65] Z. Ying, G. Li, Y. Ren, R. Wang, and W. Wang, "A new image contrast enhancement algorithm using exposure fusion framework," in *Proc. Comput. Anal. Images Patterns*, 2017, pp. 36–46.
[66] X. Ren, M. Li, W. H. Cheng, and J. Liu, "Joint enhancement and denoising method via sequential decomposition," in *Proc. Comput. Vis. Pattern Recognit.*, May 2018, pp. 1–5.

VIACHESLAV VORONIN (Member, IEEE) received the B.S. and M.S. degrees in the communication system from the South-Russian State University of Economics and Service in 2006 and 2008, respectively, and the Ph.D. degree in technics from Southern Federal University in 2009. He is currently the Head of the Center for Cognitive Technology and Machine Vision at Moscow State University of Technology "STANKIN," Moscow, Russia. His research interests include image processing, inpainting, and computer vision. He is a member of the Program Committee of the conference SPIE.

ALEKSANDER ZELENSKY received the B.S. and M.S. degrees in communication system from the South-Russian State University of Economics and Service in 2005 and 2007, respectively, and the Ph.D. degree in technics from Novocherkassk Polytechnic University in 2010. He is currently the Vice-Rector for research and science and technology policy with the Moscow State University of Technology "STANKIN," Moscow, Russia. He has authored more than 60 scientific articles. His research interests include collaborative robotics, control systems, and computer vision.

SOS AGAIAN (Fellow, IEEE) received the M.S. degree *(summa cum laude)* in mathematics and mechanics from Yerevan University, Armenia, the Ph.D. degree in math and physics from the Steklov Institute of Mathematics, Russian Academy of Sciences, and the Doctor of Engineering Sciences degree from the Institute of the Control System, Russian Academy of Sciences. He is currently a Distinguished Professor with the Department of Computer Science, The CUNY Graduate Center, New York, USA. He has authored more than 700 scientific articles and ten books. He holds 54 patents/disclosures. His research interests are multimedia processing, imaging systems, information security, artificial intelligent, computer vision, 3-D imaging sensors, and biomedical and health informatics. He is Fellow of the International Society for Photo-Optical Instrumentations Engineers, the Society for Imaging Science and Technology (IS&T), and the Science Serving Society (AAAS). He also serves as a Foreign Member for the Armenian National Academy. He was a recipient of MAEStro Educator of the Year, supported by the Society of Mexican American Engineers and Scientists. The technologies he invented have been adopted across multiple disciplines, including the U.S. government, and commercialized by the industry. He is an Editorial Board Member of the *Journal of Pattern Recognition and Image Analysis* and an Associate Editor for several journals, including the *Journal of Electronic Imaging* (SPIE, IS&T), the IEEE TRANSACTIONS ON IMAGE PROCESSING, and the IEEE TRANSACTIONS ON SYSTEM, MAN, AND CYBERNETICS.